Emergency Radiology (2018) 25:533–545
https://doi.org/10.1007/s10140-018-1616-9

REVIEW ARTICLE

New and emerging patient-centered CT imaging and image-guided treatment paradigms for maxillofacial trauma

David Dreizin [1] · Arthur J Nam [2] · Jeffrey Hirsch [3] · Mark P Bernstein [4]

Received: 13 May 2018 / Accepted: 30 May 2018 / Published online: 20 June 2018

Abstract

This article reviews the conceptual framework, available evidence, and practical considerations pertaining to nascent and emerging advances in patient-centered CT-imaging and CT-guided surgery for maxillofacial trauma. These include cinematic rendering—a novel method for advanced 3D visualization, incorporation of quantitative CT imaging into the assessment of orbital fractures, low-dose CT imaging protocols made possible with contemporary scanners and reconstruction techniques, the rapidly growing use of cone-beam CT, virtual fracture reduction with design software for surgical pre-planning, the use of 3D printing for fabricating models and implants, and new avenues in CT-guided computer-aided surgery.

Keywords Maxillofacial trauma · Facial fractures · Midface · Mandible · Volume rendering (VR) · Cinematic rendering (CR) · Quantitative imaging · Volumetric analysis · Low-dose CT · Cone-beam CT · Computer-aided design (CAD) · 3D printing · Computer-aided surgery (CAS)

Introduction

Several advances in CT imaging and image-guided treatment stand to dramatically improve the care of patients with maxillofacial trauma. These include technological improvements in 3D volume rendering; advances in semi-automated segmentation for orbital volumetric measurements; improvements in CT hardware and reconstruction algorithms allowing image acquisition at doses that are orders of magnitude lower than with conventional imaging protocols; widespread and still rapidly growing implementation of inexpensive ultra-high resolution cone-beam CT units; the potential and early use of computer-aided design software for operative pre-planning, rapid prototyping of implants, and maxillofacial models as surgical aids; and incorporation of virtually repaired CT datasets into the workflow of navigational computer-aided surgery. The potential future role of radiologists as these advances are put into practice is also discussed.

✉ David Dreizin
daviddreizin@gmail.com

[1] Trauma and Emergency Radiology, Department of Diagnostic Radiology and Nuclear Medicine, R Adams Cowley Shock Trauma Center, University of Maryland Medical Center, 22 S Greene St, Baltimore, MD 21201, USA

[2] Division of Plastic Surgery, University of Maryland School of Medicine, 22 S Green St., Baltimore, MD 21201, USA

[3] Department of Diagnostic Radiology and Nuclear Medicine, University of Maryland Medical Center, 22 S Greene St, Baltimore, MD 21201, USA

[4] Division of Trauma and Emergency Imaging, Department of Radiology, Bellevue Hospital/NYU Langone Medical Center, New York, NY 10016, USA

3D volume visualization

Conventional techniques

The use of volume rendering for facial trauma has been advocated for decades. The technique commonly employed today was initially developed for medical imaging through a collaboration between Pixar and radiologists at Johns Hopkins Hospital [1, 2]. Conventional volume rendering uses traditional ray-tracing techniques, wherein scatter effects from a limited number of modeled light sources are used to create local gradient shading, and each voxel is assigned a color and opacity value based on pre-defined attenuation threshold levels for each modeled light ray [3, 4]. Until recently, improvements in the quality of 3D reconstructions have been modest and

incremental, and mostly the result of gradual reductions in section thickness and voxel size which improve anatomic detail [5, 6].

Volume rendering can mask important pathology, which requires mental integration of the 3D images with axial and MPR images [5, 7–9]. The floor of the orbit and the medial orbital wall, especially along the lamina papyracea, are typically poorly appreciated using 3D imaging, appearing at best as a latticework studded with holes [8, 9]. The thin bones of the internal orbit are of considerably lower attenuation than other bony structures, and capturing these structures is particularly challenging with conventional 3D volume-rendering algorithms. While assessment of the midfacial subunits is often greatly augmented using 3D visualization, conventional techniques are inherently limited for the evaluation of zygomatico-maxillary complex (ZMC) and naso-orbito-ethmoidal (NOE) fractures, both frequent components of Le Fort level II or III fractures that in the great majority of patients involve the thin structures of the internal orbit [5, 9, 10]. Specifically, in addition to involving the zygomatico-maxillary buttress and the zygomatico-frontal, zygomatico-temporal, and zygomatico-sphenoid sutures, ZMC fractures involve the orbital floor, and for this reason are often referred to as orbitozygomatic fractures [10]. True NOE fractures are diagnosed by identifying five "cardinal tracts," or fracture lines which form the perimeter of the central canthal-bearing NOE fragment. In addition to the orbital floor and medial wall, these involve the pyriform aperture and lateral nose, nasomaxillary buttress, and frontomaxillary suture [9] (Fig. 1). The status of soft tissue structures such as fracture dislocations of the nasal cartilage or medial canthal tendon disruptions is not well depicted in any MDCT-based modality currently in use for facial trauma [8], and require inference based on bony fracture pattern, direct visualization, or palpation and digital traction.

"Shedding new light" on 3D imaging using cinematic rendering

Cinematic rendering (CR) is a novel and recently introduced volume visualization tool developed by Siemens (Siemens AG, Forscheim, Germany), representing a new generation of volumetric imaging. Its namesake refers to implementation of sophisticated modeling used in contemporary animated movies, while harkening back to the original Pixar collaboration [3].

Instead of local gradient shading achieved with traditional ray tracing, CR uses a "global illumination model" in which real-time random sampling computational algorithms and Monte Carlo simulations are used to model the propagation of billions of different paths of high dynamic range light from all possible directions through a volumetric dataset, taking into account interactions such as light scatter, reflection, and extinction resulting from neighboring voxels. This emulates the complex physics of natural lighting effects, thereby enhancing depth and shape perception, and generating "photorealistic" images that more clearly depict bone and soft tissue detail in CT data [3, 4, 7, 11]. The more complex light modeling could potentially improve visualization of thin and low-attenuating structures including the medial wall and floor of the internal orbit (Figs. 2 and 3), as well as improving visualization of non- or minimally displaced fractures through these structures, and soft tissue structures of critical importance in facial fractures. For example, the status of the medial canthal tendon (MCT), which attaches to the anterior and posterior lacrimal crests, is a major determinant of esthetic and functional outcome after NOE fractures. The MCT is formed from the convergence and fusion of the tarsal plates. Dissociation of the MCT along with or independently from a single or comminuted NOE fragment results in telecanthus and blunting of the palpebral fissure. Assessment of the thin soft tissue structures of the tarsal plates is quite difficult with conventional VR (Fig. 4a). Cinematic rendering on the other hand improves exquisite soft tissue detail and can display these structures to advantage (Fig. 4b). Validation will be needed for this nascent technology. Additionally, CR is presently not as instantaneous as traditional volume rendering due to the computational power required and would therefore be difficult to incorporate into the radiology workflow. However, with improved capture of low-attenuating structures such as the thin bones of the orbit, CR could in the future potentially serve as a stand-alone diagnostic tool for some maxillofacial traumas, resulting in both improved accuracy and efficiency. It is already well known that surgeons prefer 3D images for surgical planning, and have greater accuracy in evaluating 3D images than MPRs [6]. Improving the quality of 3D images may therefore improve planning, which could ultimately have a positive effect on surgical outcomes.

Orbital volumetry: a quantitative imaging biomarker for predicting late enophthalmos

Absence of enophthalmos on initial examination after orbital volume changes following blowout fracture does not exclude its subsequent development, as bony orbital volume expansion is initially counteracted by soft tissue swelling [12, 13]. Soft tissue swelling usually resolves by approximately 4 weeks, at which time enophthalmos becomes clinically apparent. Failure to account for this masking phenomenon can result in delayed diagnosis and inadequate treatment [14–16]. Surgical correction of late post-traumatic enophthalmos is very challenging, and satisfactory results are often not achieved [17, 18].

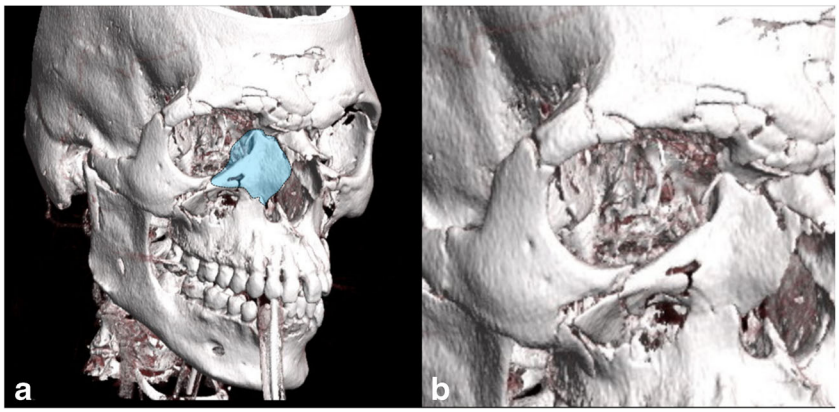

Fig. 1 A 49-year-old man after a motor vehicle collision with complex maxillofacial fractures including a right naso-orbito-ethmoidal component. On the 3D volume-rendered image (**a**), fracture lines are seen extending through the inferior orbital rim to the pyriform aperture, the nasomaxillary suture, and frontomaxillary suture (blue shading). Medial orbital wall and floor fractures, which complete the NOE fragment, are poorly visualized due to lack of depth and fragment perception (coned down image (**b**))

CT-based enophthalmos risk assessment has classically been qualitative, subjective, and imprecise—based largely on fracture location and rough estimates of defect size [19–21]. CT-based orbital volume analysis as a quantitative marker for predicting late enophthalmos was initially demonstrated in 1985 [22], is now well-validated, and may improve outcome [14, 17, 19, 23]. Each 0.8–1 cm^3 of bony volume expansion results in 1 mm of enophthalmos in a linear fashion [12, 17, 24, 25]. Once predicted enophthalmos reaches a threshold of 2–3 mm, cosmetic deformity can be expected [17].

Despite established volume-based criteria, quantitative analysis has not yet become standard practice [12]. In the past, volumetric measurement required a time-intensive manual process of slice-by-slice region of interest tracing, precluding its point-of-care use [12, 14, 19]. Versatile and rapid segmentation tools using thresholding or seeded region-growing techniques are now integrated components of commercial PACS-linked post-processing software, and can be used in daily practice to measure either differences in whole orbital volume, or the volume of tissue prolapsed through a floor or medial wall defect [12, 19] (Fig. 5). Intra- and inter-operator errors with these techniques are low when using thin-section datasets, and segmentation times are typically under 2 min. Since there is normally 7–8% of volume difference between both orbits in any given individual [19, 26], and defining the anterior boundary of the whole orbit is subjective, assessment of the volume of herniated contents could be more reliable [19, 27]. Additional improvements in automation may allow intra-operative orbital volume measurements during computer-assisted surgery, which could reduce the need for subsequent revision procedures.

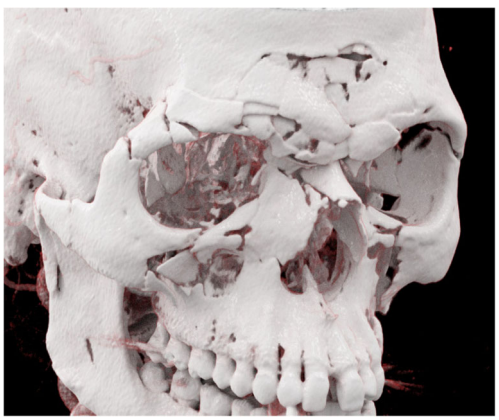

Fig. 2 A 49-year-old man after a motor vehicle collision with complex maxillofacial fractures including a right naso-orbito-ethmoidal component. Cinematic rendering 3D image shows improved depth and shape perception, greatly improving depiction of orbital floor and medial wall comminuted blowout fracture fragments

Dose reduction paradigms: low-dose, ultra-low dose, and cone-beam computed tomography

Low-dose and ultra-low-dose CT

While the as low as reasonably achievable (ALARA) principle is a ubiquitously familiar concept to radiologists, low-dose face CT protocols are rarely employed in the setting of trauma. The potential dose reduction is multiplicative since pre- and post-operative CT is routinely employed as the standard of care, and repeat follow-up exams are often required in challenging cases [28–30]. At this time, papers published on the topic of low-dose post-trauma maxillofacial CT have primarily involved cadaver studies [28, 29, 31]. Nevertheless, inflammatory soft tissue changes are well appreciated using widely implemented ultra-low-dose sinusitis protocols [30, 32], and it stands to reason that post-traumatic pathology including fibrofatty tissue entrapment, extra-ocular muscle herniation, or retrobulbar hematomas can also be readily appreciated. Beam-hardening effects and photon starvation from

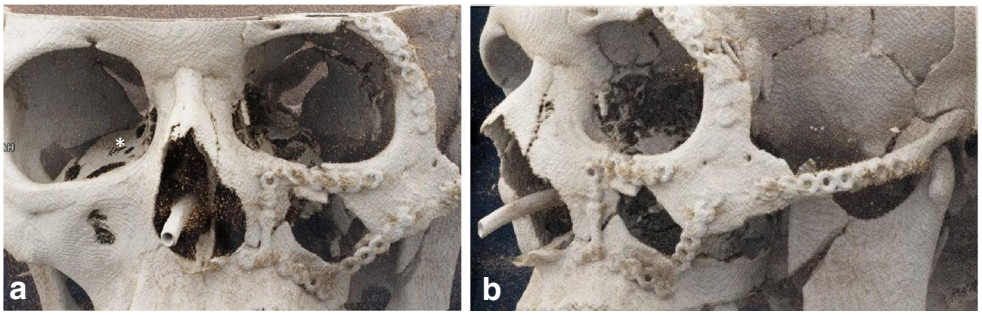

Fig. 3 A 26-year-old woman after motor vehicle collision with a high-energy comminuted left ZMC fracture. On the right, the convex posteromedial bulge of the orbit, responsible for maintaining forward projection of the globe, is well depicted on the CR reconstruction despite the very thin bone in this region (asterisk). By comparison, there is blowout of both the floor (**a**) and medial wall on the left (**b**). **b** A 26-year-old woman after motor vehicle collision with a high-energy comminuted left ZMC fracture

hardware are a potential limitation [29]; however, the plates and mesh implants used in midfacial and orbital reconstruction are very low in profile. Low dose is usually achieved using low mA settings [29, 31]. The use of image series reconstructed with both sharp (bone) and smooth (soft tissue) kernels can effectively limit metal artifact while preserving soft tissue contrast and image quality when using low-dose protocols (Fig. 6). The effects of metal artifact could potentially be further mitigated using the high-spectrum datasets from dual-energy CT with the use of a tin filter, which preferentially absorbs low-energy photons, and increases the mean energy of the X-ray spectrum [33].

The effective dose of MDCT can also be substantially reduced using contemporary 128-section or higher scanners with improved coupling of detectors and electronic components that minimize loss of signal, higher pitch, automated tube current modulation, and noise reduction techniques (particularly iterative reconstruction). These techniques can be used to create low-dose protocols with effective doses close to 0.1 mSv (within the range of cone-beam CT), and well below multiple-view plain radiographic series, while maintaining excellent soft tissue detail and accuracy for detection of non-displaced fractures [28, 29, 31, 34–36].

Cone-beam CT

Although primarily used for orthodontics at this time, cone-beam CT (CBCT) is emerging as an easily accessible modality with several important applications in maxillofacial trauma [37], particularly for diagnosing simple mandibular fractures or dentoalveolar trauma in an outpatient/walk-in clinic setting [38, 39], where cost, access, and availability of MDCT, which requires a dedicated imaging department, are prohibitive [40, 41].

CBCT was developed in 1982 and introduced commercially in 2001 [39]. In the intervening years, the modality has rapidly evolved along with the increased data processing power of personal computers [37]. Unlike MDCT, in which tube and multidetector row pairs acquire data using spiral slip-ring technology, CBCT scanners incorporate a cone-shaped X-ray

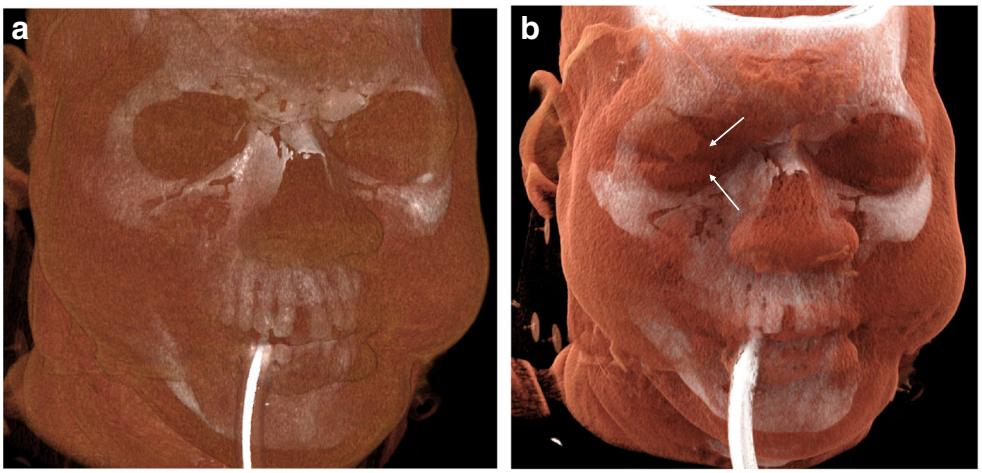

Fig. 4 **a** A 49-year-old man after motor vehicle collision with complex maxillofacial fractures including a right naso-orbito-ethmoidal component, previously shown in Figs. 1 and 2. Conventional volume rendering with soft tissue windowing poorly depicts the tarsal plates of the eyelids, which converge to form the medial canthal tendon. **b** Cinematic rendering depicts the tarsal plates as discrete structures. In this case, lateral deviation of the tarsal plates is evident (arrows), consistent with telecanthus, providing additional potentially valuable information for both grading of NOE fracture severity and pre-operative planning

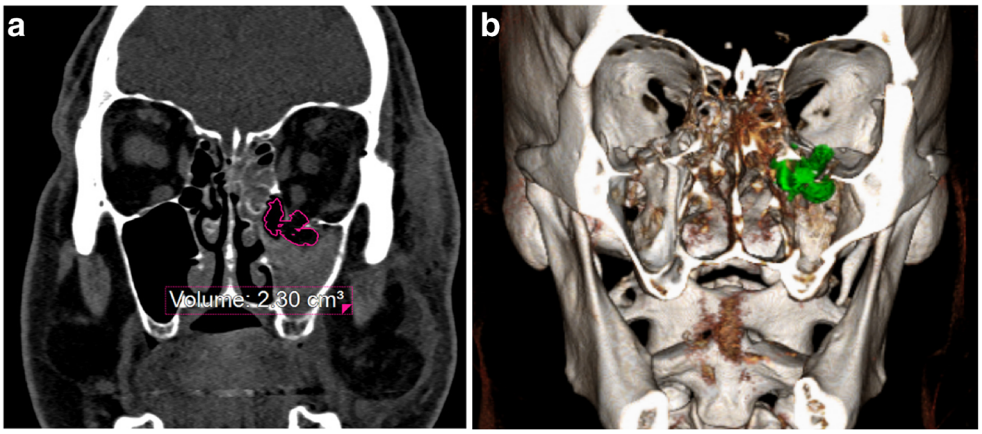

Fig. 5 **a** Segmentation using semi-automated seeded region growing was performed in under 1 min in this 54-year-old man with a left orbital blowout fracture after being hit by a tree limb. The volume of prolapsed fat placed the patient at high risk for the development of enophthalmos, and the orbital floor was reconstructed with a titanium implant. **b** 3D VR image of the same patient as shown in Fig. 4a displays the segmented volume of prolapsed left orbital contents in its entirety

beam (instead of a collimated fan beam) incident on a single flat-panel detector. Data is acquired in a single rotation of a free-standing unit, and reconstructed into series of cross-sectional images using a process of back-transformation similar to that of MDCT [42, 43]. Images are displayed in multiplanar cross-sectional reconstructions; 3D post-processing techniques including curved planar reformats (CPRs) for mandibular panoramic images, maximum-intensity projection images (MIPs), and surface-rendered techniques are easily employed on a standard PC workstation with very short reconstruction times [37, 40, 41] (Fig. 7).

Contemporary MDCT scanners can provide truly isotropic datasets depending on the scanner settings used, and ultra-high-resolution section thicknesses of 0.4 mm can now be achieved. CBCT datasets on the other hand are inherently isotropic, consisting of voxel sizes typically ranging from 0.075 μm to 0.5 mm, depending on the field of view and scanner specifications. While radiation dose varies considerably between different CBCT scanners, and settings or specifications including fields of view, CBCT is typically associated with much lower radiation doses (in the micro-Sievert range) compared with conventional MDCT protocols, on the order of one magnitude of difference in effective dose [37, 41, 42]. However, this comes at the expense of poor soft tissue contrast, the inability to accurately measure Hounsfield units, and susceptibility to motion artifact due to relatively long scan

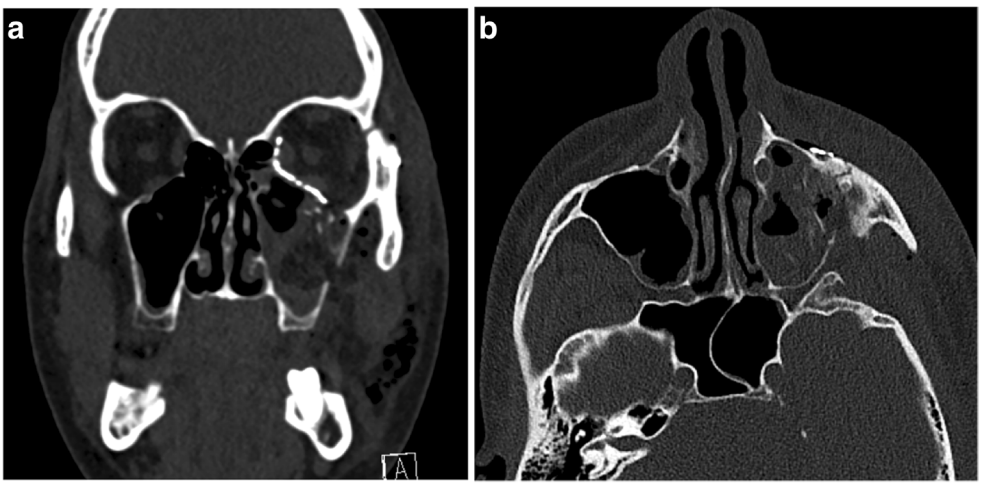

Fig. 6 **a** CT following internal orbital reconstruction in a 24-year-old man who sustained an orbital blowout fracture after a motor vehicle collision. Images were acquired using a low-dose protocol at 20 mAs and 100 kVp. A soft tissue kernel was employed using a state-of-the-art dual-source 128-detector row scanner (Br40, Siemens Force; Siemens AG, Forscheim, Germany), which maintained excellent soft tissue contrast within the orbital contents, clearly displaying the optic nerve and extra-ocular muscles as distinct well-defined structures surrounded by fibrofatty tissue. There is very little artifact associated with the orbital implant. **b** CT following internal orbital reconstruction in a 24-year-old man who sustained an orbital blowout fracture after a motor vehicle collision. Images were acquired using a low-dose protocol at 20 mAs and 100 kVp (same patient as shown in **a**). Images were also reconstructed using a bone kernel (Br64) to maximize bony detail. Hairline fractures at the left orbital rim are clearly depicted using the bone algorithm, while soft tissue contrast is poor

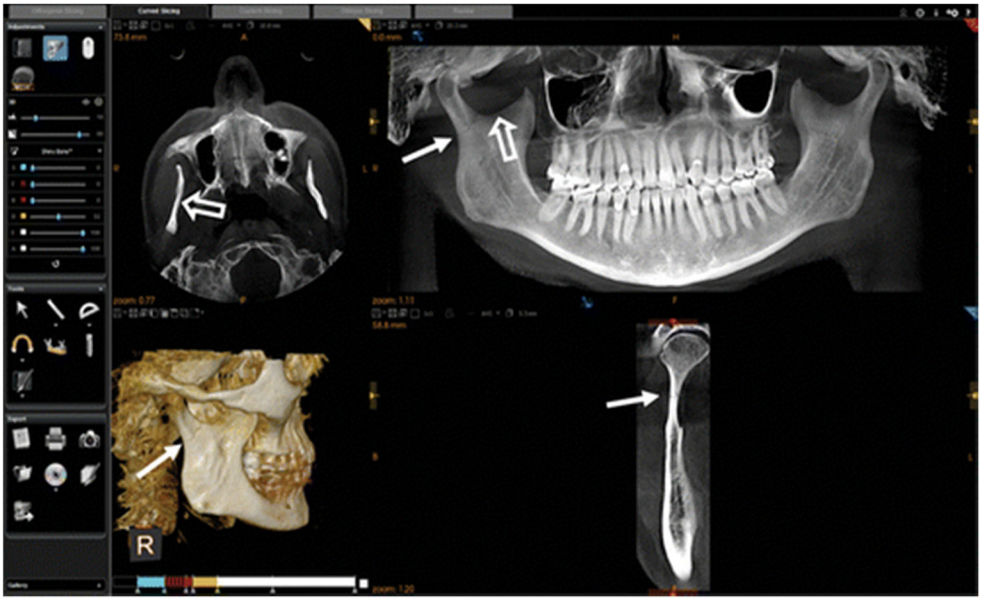

Fig. 7 Images obtained in a 60-year-old woman with jaw pain after a fall from standing. Cone-beam CT was performed by using a medium field-of-view scanner (Carestream 9300 3D; Carestream Dental, Atlanta, GA). A screen capture of images obtained by using three-dimensional software highlights the volume visualization capabilities and ultra-high resolution of cone-beam CT. Axial thick cone-beam CT image with multiplanar reformation (*top left*), curved planar cone-beam CT image with reformation of the mandible (*top right*), three-dimensional volume-rendered image (*bottom left*), and coronal oblique cone-beam CT image obtained along the long axis of the right condyle (*bottom right*) are shown. Solid arrows point to the hairline right subcondylar fracture at the level of the sigmoid notch (open arrow in the axial [*top left*] and curved planar [*top right*] images). Figure and caption (with permission from author and publisher) from Dreizin et al. "Multidetector CT of mandibular fractures, reductions, and complications: a clinically relevant primer for the radiologist." *RadioGraphics* 36.5 (2016), pp. 1539–1564 [43]

times. Since most CBCT units require the patient to sit in an upright position, and intravenous contrast is not used, CBCT has limited utility for polytraumatized patients [43].

While upright units are now in widespread use, early prototypes included mobile CBCT c-arms designed to confirm reduction of midfacial fractures while the patient is still on the operating table, potentially reducing the rate of unnecessary reoperation; however, visualization of thin structures such as the medial orbital wall remains difficult, especially in osteopenic patients, and soft tissue contrast is again poor [39, 44, 45]. Mobile intra-operative MDCT is now being used for craniofacial applications, and can overcome these limitations, but units are costly and associated with high radiation dose [46, 47].

Computer-aided design, manufacturing, and surgery: emergence of a fully digital workflow

CAD/CAM software for virtual pre-operative planning and rapid prototyping

3D modeling with computer-aided design and computer-aided manufacturing (CAD/CAM) software can be used to perform digital manipulations to "virtually reduce" segmented fracture fragments into pre-morbid or near-pre-morbid alignment, either for pre-operative planning, rapid prototyping, or both [46, 48, 49]. Pre-operative planning and rapid prototyping using design software is becoming increasingly intuitive, efficient, and precise, particularly for internal orbital reconstruction, and can potentially decrease operative time and difficulty while improving esthetic results [50]. Because of the delicate and complex sloping anatomy of the internal orbit, high-velocity fractures with large-volume increases and collapse of the internal orbital buttress, posteromedial bulge, and posterior shelf are challenging to safely and effectively reconstruct without intra-operative navigation and computer-aided surgery (CAS) [50, 51]. Navigational CAS promotes accurate positioning of implants, which must cover the entire defect and rest on the posterior shelf [50, 52]. Mirroring of the contralateral uninjured side after segmentation is typically used to virtually restore the sloping and convex topography of the orbit. This process is becoming increasingly automated [48, 50, 51, 53], and is being combined with intra-operative navigation to more precisely restore orbital shape and volume [49, 51]. In the future, CAD/CAM reconstructions and navigation may be useful to overcorrect the orbital volume in patients with severe injury that may be at heightened risk of enophthalmos from fat atrophy [51]. Currently, the most commonly employed CAD/CAM software in the published craniomaxillofacial literature is Materialize Mimics (Materialize, Ann Arbor, MI), with

iPlan also in use (Brainlab, Westchester, IL). The most commonly used printing software is 3D-Systems (3D-systems, Valencia, CA) [54].

After a process of data transfer involving conversion of Digital Imaging and Communication in Medicine (DICOM) images into the proprietary language of the specific design software employed [40, 55, 56], using common midfacial subunit-specific surgical landmarks (such as specific sutures and buttresses), a zygomaticomaxillary complex, or naso-orbito-ethmoid fracture, can be first segmented into a distinct element and virtually repositioned into normal alignment (Fig. 8). This may more precisely reflect pre-morbid alignment than mirroring, which involves superimposition of the contralateral unaffected side across a plane through the patient's midline. Mirroring is a more rapid technique, but which does not account for inherent differences in pre-morbid facial asymmetry between sides, for which there is considerable variability between individuals [26, 51] (Fig. 9). Virtual osteotomies and repositioning can also be performed for fractures that are treated late and have become malunited [46, 51, 57]. After virtual reconstruction or mirroring, mandibular or maxillofacial models can be created through rapid prototyping (3D printing) (Figs. 10 and 11). 3D printing is a now commonly used vernacular term referring to a number of rapid-prototyping techniques. The virtual dataset can also be back-converted to DICOM format and uploaded to intra-operative CAS navigation system workstations for real-time supervision of the reduction [46, 52].

CT image-based 3D printing after maxillofacial trauma: technical principles

CT-based rapid prototyping is increasingly used for a number of applications in post-traumatic facial reconstruction [54], particularly for the creation of mandibular or midfacial models, and patient-specific orbital implants (PSIs). The World Health Organization (WHO) has called for the replacement of conventional implants with PSIs in routine practice by the year 2020 [56]. Rapid prototyping can be performed using a variety of additive or subtractive manufacturing methods. Milling is a subtractive method that employs multiaxis drills or other sharp tools. While milling saves considerable time, it is less precise and therefore not ideal for reconstructing the thin walls and surrounding cavities of the midfacial region, and is rarely used for creating maxillofacial models [58]. Additive manufacturing is the global technical standards term for 3D printing. A variety of methods can be used to create maxillofacial models including stereolithography (vat photopolymerization), material jetting, and binder jetting. A detailed description of the various techniques is beyond the scope of this article, but a comprehensive discussion is found in the 2015 RadioGraphics article, Medical 3D Printing For the Radiologist, by Mitsouras et al. [59]. Stereolithography is a relatively inexpensive 3D process most commonly used at this time to create surgical models in maxillofacial trauma and involves solidifying selected areas within a vat of photocurable liquid acrylic resin using an ultraviolet laser (see Figs. 10 and 11). The prototyping process is performed in a slice-by-slice fashion, using points triangulated by the CAD design to recreate the fine bony contour of the maxillofacial model [40, 55, 58]. Scaffolds are added to the CAD design to prevent movement of the prototype within the liquid bath during manufacturing, and these are subsequently removed. After an additional curing step using an ultraviolet oven to improve the mechanical properties of the model, the prototype can then be used to pre-bend plates or serve as a template for manual or pressure unit-based orbital implant molding [51, 58, 60]. Material jetting is a versatile technique analogous to ink-jet printing; printers spray layers of the model using two or more jetting heads for the model and a gel or wax-like support material which is subsequently removed by a combination of soaking the model in a mild soap solution, heating, or water-blasting [59]. Binder jetting also uses a jetting head, which sprays a binding material to selectively bond a powder in layers [59]. Material and binder jetting methods can be used to create color-coded models.

Another 3D printing process—laser sintering—incorporates a high-powered (typically carbon dioxide-based) laser to fuse small particles within a powder, which is applied, heated, and bonded in successive layers [56, 61]. This technique is used by vendors to create titanium orbital PSIs for surgical use (Fig. 12). Orbital implants created using selective laser sintering are generally thicker than conventional mesh implants and require precise pre-operative planning, but appear to be superior in precision, time effort, and outcome to manually bent implants [56, 62].

CT image-based 3D printing and surgical pre-planning using design software: practical considerations

A number of vendors provide comprehensive services for rapid prototyping and pre-planning based on pre-operative CT images, including offering interactive web-based meetings (typically during regular business hours) between surgeons and the vendors' software engineers or other non-medical staff who perform virtual manipulations under the direction and to the specifications of the surgeon [54, 61]. The average time to create a printed object in the published literature is approximately 19 h, and the average cost approximately 1400 US dollars, but may run much higher depending on overhead and the billing practices of the service provider. Depending on the location of the vendor, delays in receiving the model or implant can be longer than 1 week [54, 60, 61]. Costs and time can be substantially reduced through in-house pre-planning and model design using commercially available or open-source software, and either using on-site printing, or through

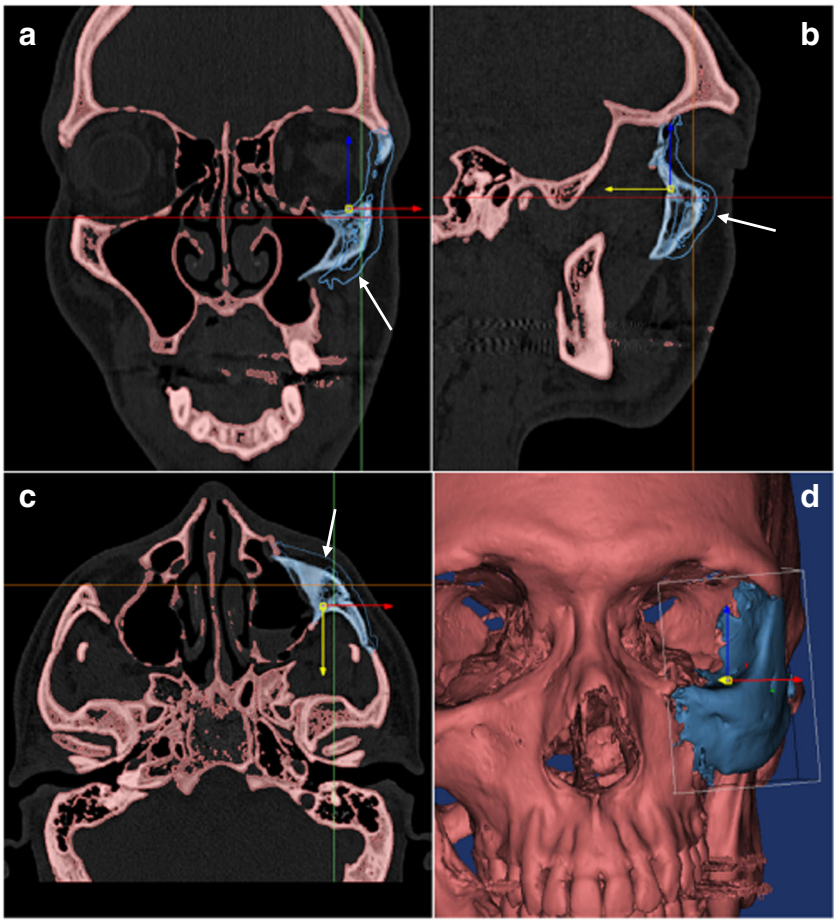

Fig. 8 A 46-year-old man who sustained a left ZMC fracture after falling down stairs. Collage shows repositioning of the ZMC using Materialize Mimics 3D modeling software. The initial ZMC fracture resulted in malar retrusion (i.e., posterior displacement with loss of facial antero-posterior projection), and medial rotation, resulting in loss of facial width. In **a**–**c**, the blue mask highlights the segmented ZMC, while the contours (arrows) show the position after virtual reduction. A key element of ZMC reduction is alignment of the zygomaticosphenoid suture along the lateral orbital wall, which is confirmed on the 3D volumetric image shown in **d**

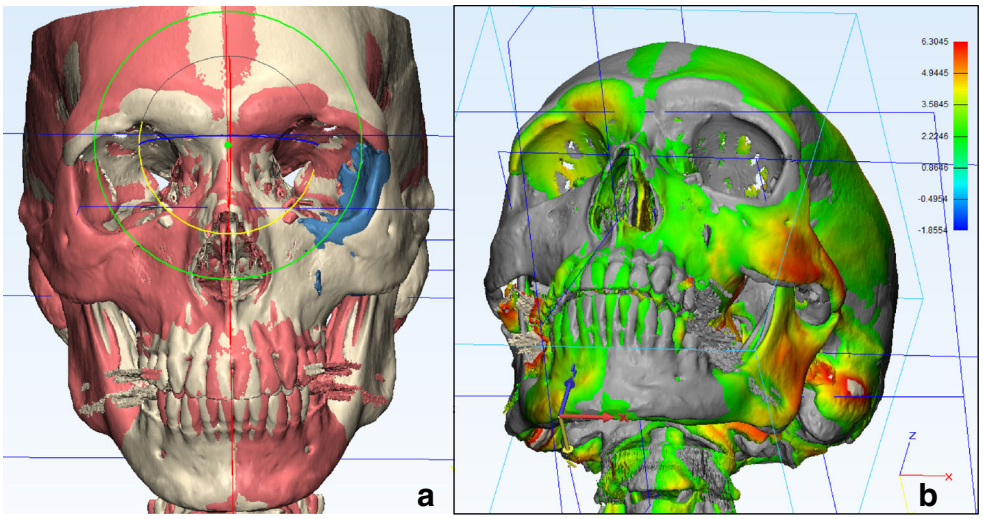

Fig. 9 Materialize 3Matic CAD software was used to mirror the intact right face onto the left in the same patient following conversion of the virtual left ZMC reduction from DICOM to STL (standard tessellation language) format (**a**). Color histogram in **b** shows differences in position between mirroring and virtual reduction, with areas of red shading corresponding with differences of greater than 5 mm from the outer edge of the reconstructed and mirrored ZMC and the mirrored versus native intact mandible. The histogram illustrates the inherent differences in pre-morbid facial symmetry, not accounted for when using the mirroring technique

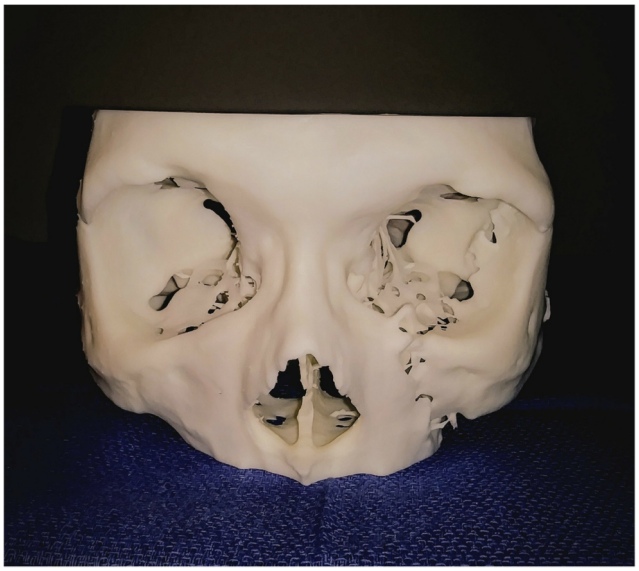

Fig. 10 Stereolithographic maxillofacial model of the same patient shown in Figs. 8 and 9 following virtual reduction of the left ZMC. The fracture lines are conspicuous, but the model shows restored facial projection and symmetry

collaborative agreements with academic institutions that have invested the necessary resources to streamline production of models or implants. In experienced hands, CT data processing and manipulation is rapid, and model generation takes approximately 8–12 h [60]. Presently, a major barrier to widespread implementation is the lack of a stand-alone process for reimbursement. Vendors providing rapid-prototyping and preplanning services are sometimes paid indirectly through contracts with medical device manufacturers that bill third-party payers in a single bundled medical device fee [63]. As interest grows, an increasing number of providers shoulder the cost as an out-of-pocket expense. Third-party payers currently do not reimburse for rapid prototyping by in-house 3D facilities, and support at major academic centers comes mainly from internal research and development grants [63].

CT-guided CAS: technical principles

Intra-operative navigation systems triangulate and track the coordinates of both the patient and instruments in space after an initial process of intra-operative surface registration which synchronizes true coordinates to the CT dataset [64, 65]. After registration, both the patient and surgical instruments can be moved freely in space [64, 65]. Both optical and electromagnetic tracking systems are in use, with the former more widely employed [64]. Passive optical navigation systems are comprised of a camera mount with an infrared emitter and high-precision receivers that track input from a reference arc attached to a rigidly fixed headset and surgical instruments, both equipped with reflective marker spheres (Fig. 13). Active tracking systems employ the same basic principles, but track coordinates through signal received from light-emitting diodes (LEDs) [46, 64, 65]. Frameless systems using LEDs attached to an adhesive mask have also been introduced [51]. The patient and instrument coordinates are co-registered to the CT data and displayed in real time, with refresh rates of up to 30 frames/s, in three planes along with 3D reconstructions on the CAS monitor with a registration error typically just over 1 mm [46, 65]. The virtually reconstructed images created using CAD/CAM software can potentially be uploaded to the CAS workstation along with the pre-operative images to guide the fractured midface segment reduction using a pointer co-registered to both datasets, from its post-traumatic alignment to its virtually restored anatomic alignment with continuously updated information. In this way, despite visualization of the fracture typically being restricted to a limited number of cosmetically favorable incision sites, the surgeon can scan the pointer over the bone surface to repeatedly assess that the repair precisely matches the planned outcome [46, 48, 51]. In some cases, the immediate evaluation of reduction during surgery can potentially obviate the need for post-operative CT scan [46, 50].

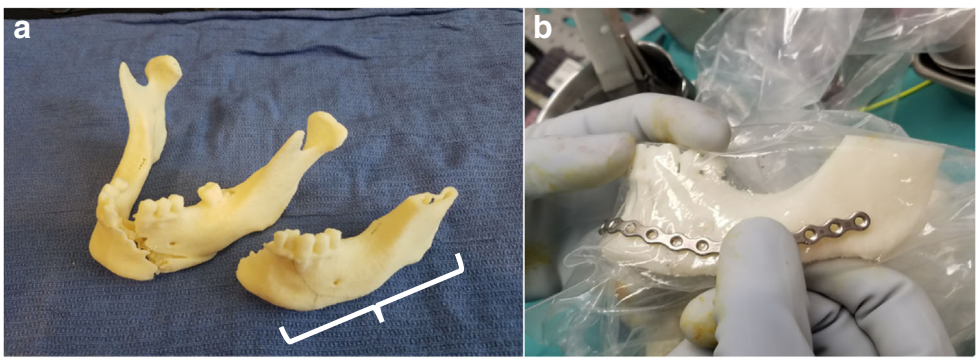

Fig. 11 **a** A stereolithographic model of a mandible segmented from the admission maxillofacial CT of a 51-year-old patient following a motorcycle collision. There is a fracture of the left symphysis-body junction. A model of the mirrored unaffected right side (bracket (**a**)) and **b** was used to pre-bend an inferior border reconstruction plate. 3D printed models can be used as a frame of reference for the surgical reduction and as templates for pre-bending titanium plates pre-operatively to potentially improve the surgical result while decreasing operative time

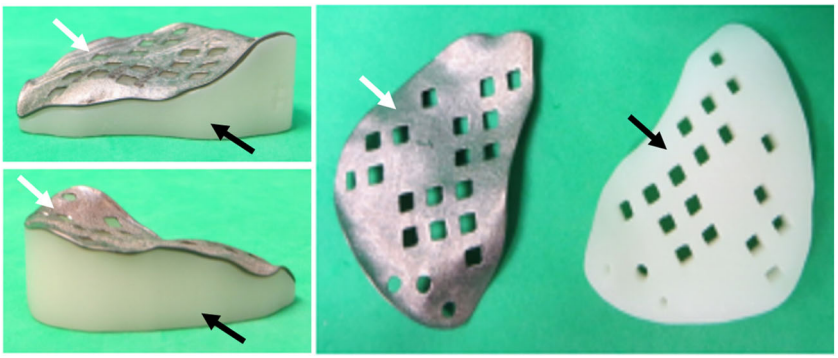

Fig. 12 Patient-specific sintered titanium implant (white arrows) on top of a 3D-printed template (black arrows) used for orbital reconstruction in a 73-year-old woman with a right orbital blowout fracture after a fall. The template and implant were manufactured from the pre-operative CT using computer-aided design to mirror the unaffected left orbit

Computer-aided surgery: growing utility for facial trauma reconstruction

CT-guided navigation surgery was initially introduced in the late 1980s for intra-operative localization of intra-cranial tumors [50, 66], and is now used for most intra-cranial neurosurgical procedures as well as for functional endoscopic sinus surgery and skull-based surgery [67, 68]. CAS is cost, resource, and personnel intensive, which creates barriers to its non-elective use in the trauma setting [46, 52]. While CAS does allow safer dissection during orbital reconstruction, its early use for facial fracture reduction had limited utility because pre-operative DICOM datasets did not provide valuable information to guide reduction back into anatomic pre-morbid alignment and symmetry [48]. Imprecise qualitative comparison of symmetry to the contralateral uninjured side would have to be used. The reliance on only pre-operative data has limited the utility of CAS for precise facial fracture reduction.

Simulation of pre-planned osteotomies and reductions in malunited fractures and generation of models for the relatively imprecise interactive use as surgical aids has been possible with CAM/CAD software for some time, but only with the emerging use of virtually reconstructed datasets for providing real-time intra-operative guidance for the reduction, along with plate pre-bending with stereolithographic models, has CAS become more feasible and appealing for facial fracture reconstruction outside of the orbit [46, 49–51, 57, 69–71]. The ability to back-convert from proprietary design software format to DICOM is becoming an increasingly standard functionality of CAD/CAM applications [48, 51]. The possibility of improved esthetic and functional outcomes when using the virtual repair to represent the treatment plan in real time is particularly promising for high-velocity severely comminuted or malunited fractures of the ZMC, NOE, or maxillary occlusal regions, where surgical landmarks typically used for reduction may no longer be available due to bone loss, or altered as the result of bony remodeling [46, 48, 52, 65].

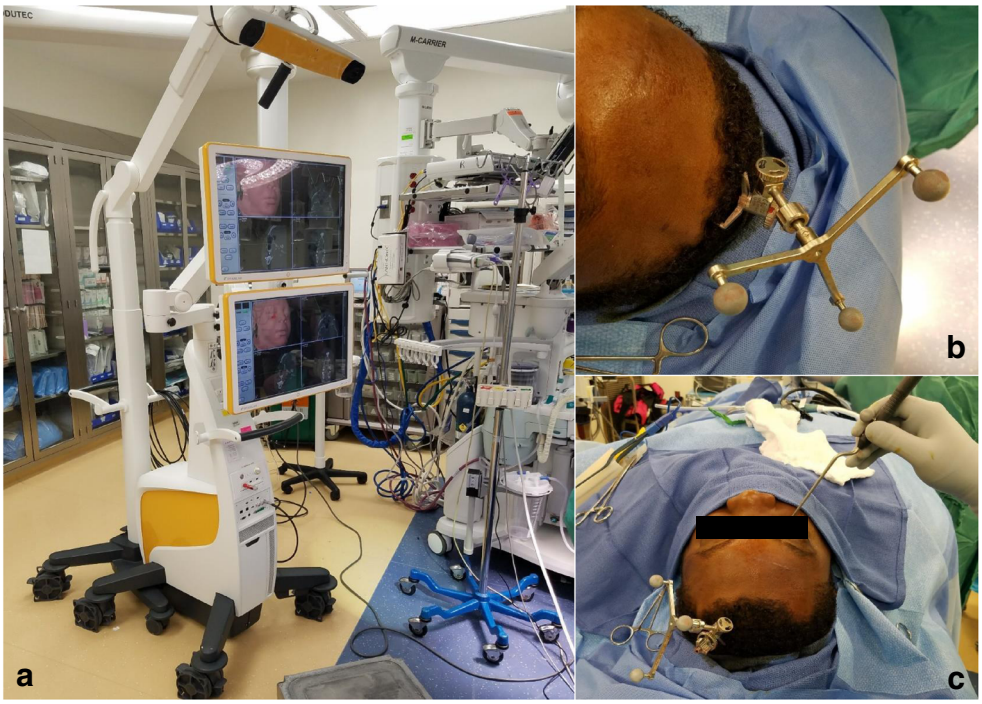

Fig. 13 CT-guided, computer-aided orbital reconstruction in a patient with orbital fracture. **a** The infrared camera and receiver mount with monitors for CT-guided navigation. A reference arc with reflective markers attached to a rigidly fixed headset is shown (**b**). Both the headset and a surgical instrument fitted with a reflective sphere are illustrated in **c**

Radiologist: virtually a craftsperson? The potential future role of radiologists in virtual surgical pre-planning and rapid prototyping

While there is a chance that without initiative and active engagement with reconstructive surgery colleagues in this area, radiologists will lose a unique opportunity to extend beyond the role of imaging consultant to collaborator in the surgical planning process and be completely circumvented in the workflow, some of the circumstances described—particularly the high cost and delays that may result with reliance on outside vendors—point to a potential future role in this capacity for imagers in establishing and making use of in-house resources and facilities. The path toward adoption and radiologist involvement will be contingent on ever-increasing demand, outcomes research to support advocacy, and the establishment of communities within the discipline, such as the recently formed Radiological Society of North America 3D Printing Special Interest Group, which is currently developing appropriateness criteria for craniomaxillofacial and other applications.

Conclusion

Potentially transformative emerging patient-centered paradigms in maxillofacial imaging and image-guided reconstruction require that radiologists challenge themselves to develop familiarity with new volume visualization tools such as the nascent technique of cinematic rendering; strive to incorporate quantitative imaging in their daily practice for prediction of enophthalmos after orbital blowout fractures; utilize advanced dose reduction strategies to minimize patient radiation exposure; and develop new skill sets while growing their institutional infrastructure to incorporate computer-aided design, virtual fracture reconstruction, and rapid prototyping.

Compliance with ethical standards

Conflict of interest David Dreizin is the recipient of a research grant from Siemens Healthineers.

References

1. Fishman EK, Drebin B, Magid D, Scott WW Jr, Ney DR, Brooker AF Jr, Riley LH Jr, St Ville JA, Zerhouni EA, Siegelman SS (1987) Volumetric rendering techniques: applications for three-dimensional imaging of the hip. Radiology 163(3):737–738
2. Catmull E, Fishman EK, Horton KM, Raman SP (2015) From toy story to CT scans: lessons from Pixar for radiology. J Am Coll Radiol 12(9):978–979
3. Fellner FA (2016) Introducing cinematic rendering: a novel technique for post-processing medical imaging data. J Biomed Sci Eng 9(03):170–175
4. Eid M et al (2017) Cinematic rendering in CT: a novel, *Lifelike 3D Visualization Technique*. Am J Roentgenol:1–10
5. Fox LA, Vannier MW, West OC, Wilson AJ, Baran GA, Pilgram TK (1995) Diagnostic performance of CT, MPR and 3DCT imaging in maxillofacial trauma. Comput Med Imaging Graph 19(5): 385–395
6. Reuben A et al A comparative study of evaluation of radiographs, CT and 3D reformatted CT in facial trauma: what is the role of 3D? Br J Radiol 2014
7. Dappa E, Higashigaito K, Fornaro J, Leschka S, Wildermuth S, Alkadhi H (2016) Cinematic rendering–an alternative to volume rendering for 3D computed tomography imaging. Insights into Imaging 7(6):849–856
8. Saigal K, Winokur RS, Finden S, Taub D, Pribitkin E (2005) Use of three-dimensional computerized tomography reconstruction in complex facial trauma. Facial Plast Surg 21(03):214–220
9. Remmler D, Denny A, Gosain A, Subichin S (2000) Role of three-dimensional computed tomography in the assessment of nasoorbitoethmoidal fractures. Ann Plast Surg 44(5):553–563
10. Mehta N, Butala P, Bernstein MP (2012) The imaging of maxillofacial trauma and its pertinence to surgical intervention. Radiol Clin North Am 50(1):43–57
11. Johnson PT et al (2017) MDCT angiography with 3D rendering: a novel cinematic rendering algorithm for enhanced anatomic detail. Am J Roentgenol:1–4
12. Strong EB, Fuller SC, Chahal HS (2013) Computer-aided analysis of orbital volume: a novel technique. Ophthal Plast Reconstr Surg 29(1):1–5
13. Manson PN, Grivas A, Rosenbaum A, Vannier M, Zinreich J, Iliff N (1986) Studies on enophthalmos: II. The measurement of orbital injuries and their treatment by quantitative computed tomography. Plast Reconstr Surg 77(2):203–214
14. Raskin EM et al *Prediction of late enophthalmos by volumetric analysis of orbital fractures*. 1998. LWW
15. Hawes MJ, Dortzbach RK (1983) Surgery on orbital floor fractures: influence of time of repair and fracture size. Ophthalmology 90(9): 1066–1070
16. Dreizin D, Nam AJ, Diaconu SC, Bernstein MP, Bodanapally UK, Munera F (2018) Multidetector CT of Midfacial fractures: classification systems, principles of reduction, and common complications. RadioGraphics 38(1):248–274
17. Fan X, Li J, Zhu J, Li H, Zhang D (2003) Computer-assisted orbital volume measurement in the surgical correction of late enophthalmos caused by blowout fractures. Ophthal Plast Reconstr Surg 19(3):207–211
18. Grant MP, Iliff NT, Manson PN (1997) Strategies for the treatment of enophthalmos. Clin Plast Surg 24(3):539–550
19. Ploder O, Klug C, Backfrieder W, Voracek M, Czerny C, Tschabitscher M (2002) 2D-and 3D-based measurements of orbital floor fractures from CT scans. J Craniomaxillofac Surg 30(3):153–159
20. Jin H-R, Shin SO, Choo MJ, Choi YS (2000) Relationship between the extent of fracture and the degree of enophthalmos in isolated blowout fractures of the medial orbital wall. J Oral Maxillofac Surg 58(6):617–620
21. Gilbard SM, Mafee MF, Lagouros PA, Langer BG (1985) Orbital blowout fractures the prognostic significance of computed tomography. Ophthalmology 92(11):1523–1528
22. Bite U, Jackson IT, Forbes GS, Gehring DG (1985) Orbital volume measurements in enophthalmos using three-dimensional CT imaging. Plast Reconstr Surg 75(4):502–507
23. Diaconu SC, Dreizin D, Uluer M, Mossop C, Grant MP, Nam AJ (2017) The validity and reliability of computed tomography orbital volume measurements. J Craniomaxillofac Surg 45:1552–1557

24. Lee J, Chiu H (1993) Quantitative computed tomography for evaluation of orbital volume change in blow-out fractures. J Formos Med Assoc= Taiwan yi zhi 92(4):349–355
25. Whitehouse R et al (1994) Prediction of enophthalmos by computed tomography after "blow out" orbital fracture. Br J Ophthalmol 78(8):618–620
26. Forbes G, Gehring DG, Gorman CA, Brennan MD, Jackson IT (1985) Volume measurements of normal orbital structures by computed tomographic analysis. Am J Roentgenol 145(1):149–154
27. Deveci M, Öztürk S, Şengezer M, Pabuşcu Y (2000) Measurement of orbital volume by a 3-dimensional software program: an experimental study. J Oral Maxillofac Surg 58(6):645–648
28. Widmann G, Dalla Torre D, Hoermann R, Schullian P, Gassner EM, Bale R, Puelacher W (2015) Ultralow-dose computed tomography imaging for surgery of midfacial and orbital fractures using ASIR and MBIR. Int J Oral Maxillofac Surg 44(4):441–446
29. Widmann G, Bischel A, Stratis A, Kakar A, Bosmans H, Jacobs R, Gassner EM, Puelacher W, Pauwels R (2016) Ultralow dose dentomaxillofacial CT imaging and iterative reconstruction techniques: variability of Hounsfield units and contrast-to-noise ratio. Br J Radiol 89(1060):20151055
30. Schell B, Bauer RW, Lehnert T, Kerl JM, Hambek M, May A, Vogl TJ, Mack MG (2011) Low-dose computed tomography of the paranasal sinus and facial skull using a high-pitch dual-source system—first clinical results. Eur Radiol 21(1):107–112
31. Moritz JD, Hoffmann B, Sehr D, Keil K, Eggerking J, Groth G, Caliebe A, Dischinger J, Heller M, Bolte H (2012) Evaluation of ultra-low dose CT in the diagnosis of pediatric-like fractures using an experimental animal study. Korean J Radiol 13(2):165–173
32. Bulla S, Blanke P, Hassepass F, Krauss T, Winterer JT, Breunig C, Langer M, Pache G (2012) Reducing the radiation dose for low-dose CT of the paranasal sinuses using iterative reconstruction: feasibility and image quality. Eur J Radiol 81(9):2246–2250
33. Marin D, Boll DT, Mileto A, Nelson RC (2014) State of the art: dual-energy CT of the abdomen. Radiology 271(2):327–342
34. Kyriakou Y, Kolditz D, Langner O, Krause J, Kalender W (2011) Digital volume tomography (DVT) and multislice spiral CT (MSCT): an objective examination of dose and image quality. RoFo: Fortschritte auf dem Gebiete der Rontgenstrahlen und der Nuklearmedizin 183(2):144–153
35. Silva AC, Lawder HJ, Hara A, Kujak J, Pavlicek W (2010) Innovations in CT dose reduction strategy: application of the adaptive statistical iterative reconstruction algorithm. Am J Roentgenol 194(1):191–199
36. McCollough CH, Chen GH, Kalender W, Leng S, Samei E, Taguchi K, Wang G, Yu L, Pettigrew RI (2012) Achieving routine submillisievert CT scanning: report from the summit on management of radiation dose in CT. Radiology 264(2):567–580
37. De Vos W, Casselman J, Swennen G (2009) Cone-beam computerized tomography (CBCT) imaging of the oral and maxillofacial region: a systematic review of the literature. Int J Oral Maxillofac Surg 38(6):609–625
38. Cohenca N, Simon JH, Roges R, Morag Y, Malfaz JM (2007) Clinical indications for digital imaging in dento-alveolar trauma. Part 1: traumatic injuries. Dent Traumatol 23(2):95–104
39. Miracle A, Mukherji S (2009) Conebeam CT of the head and neck, part 2: clinical applications. Am J Neuroradiol 30(7):1285–1292
40. Scarfe WC (2005) Imaging of maxillofacial trauma: evolutions and emerging revolutions. Oral Surg Oral Med Oral Pathol Oral Radiol Endod 100(2):S75–S96
41. Shintaku WH, Venturin JS, Azevedo B, Noujeim M (2009) Applications of cone-beam computed tomography in fractures of the maxillofacial complex. Dent Traumatol 25(4):358–366
42. Tsiklakis K, Donta C, Gavala S, Karayianni K, Kamenopoulou V, Hourdakis CJ (2005) Dose reduction in maxillofacial imaging using low dose cone beam CT. Eur J Radiol 56(3):413–417
43. Dreizin D, Nam AJ, Tirada N, Levin MD, Stein DM, Bodanapally UK, Mirvis SE, Munera F (2016) Multidetector CT of mandibular fractures, reductions, and complications: a clinically relevant primer for the radiologist. RadioGraphics 36(5):1539–1564
44. Heiland M, Schulze D, Rother U, Schmelzle R (2004) Postoperative imaging of zygomaticomaxillary complex fractures using digital volume tomography. J Oral Maxillofac Surg 62(11): 1387–1391
45. Schulze D et al Radiation exposure during midfacial imaging using 4-and 16-slice computed tomography, cone beam computed tomography systems and conventional radiography. Dentomaxillofacial Radiol 2014
46. Westendorff C, Gulicher D, Dammann F, Reinert S, Hoffmann J (2006) Computer-assisted surgical treatment of orbitozygomatic fractures. J Craniofac Surg 17(5):837–842
47. Stanley RB (1999) Use of intraoperative computed tomography during repair of orbitozygomatic fractures. Arch Facial Plast Surg 1(1):19–24
48. Pham AM, Rafii AA, Metzger MC, Jamali A, Strong BE (2007) Computer modeling and intraoperative navigation in maxillofacial surgery. Otolaryngol Head Neck Surg 137(4):624–631
49. Morrison CS, Taylor HO, Sullivan SR (2013) Utilization of intraoperative 3D navigation for delayed reconstruction of orbitozygomatic complex fractures. J Craniofac Surg 24(3):e284–e286
50. Andrews BT, Surek CC, Tanna N, Bradley JP (2013) Utilization of computed tomography image-guided navigation in orbit fracture repair. Laryngoscope 123(6):1389–1393
51. Bell RB, Markiewicz MR (2009) Computer-assisted planning, stereolithographic modeling, and intraoperative navigation for complex orbital reconstruction: a descriptive study in a preliminary cohort. J Oral Maxillofac Surg 67(12):2559–2570
52. Lauer G, Pradel W, Schneider M, Eckelt U (2006) Efficacy of computer-assisted surgery in secondary orbital reconstruction. J Craniomaxillofac Surg 34(5):299–305
53. Metzger MC, Schön R, Schulze D, Carvalho C, Gutwald R, Schmelzeisen R (2006) Individual preformed titanium meshes for orbital fractures. Oral Surg Oral Med Oral Pathol Oral Radiol Endod 102(4):442–447
54. Jacobs CA, Lin AY (2017) A new classification of three-dimensional printing technologies: systematic review of three-dimensional printing for patient-specific Craniomaxillofacial surgery. Plast Reconstr Surg 139(5):1211–1220
55. Bill JS, Reuther JF, Dittmann W, Kübler N, Meier JL, Pistner H, Wittenberg G (1995) Stereolithography in oral and maxillofacial operation planning. Int J Oral Maxillofac Surg 24(1):98–103
56. Gander T, Essig H, Metzler P, Lindhorst D, Dubois L, Rücker M, Schumann P (2015) Patient specific implants (PSI) in reconstruction of orbital floor and wall fractures. J Craniomaxillofac Surg 43(1):126–130
57. He D, Li Z, Shi W, Sun Y, Zhu H, Lin M, Shen G, Fan X (2012) Orbitozygomatic fractures with enophthalmos: analysis of 64 cases treated late. J Oral Maxillofac Surg 70(3):562–576
58. Kermer C, Lindner A, Friede I, Wagner A, Millesi W (1998) Preoperative stereolithographic model planning for primary reconstruction in craniomaxillofacial trauma surgery. J Craniomaxillofac Surg 26(3):136–139
59. Mitsouras D, Liacouras P, Imanzadeh A, Giannopoulos AA, Cai T, Kumamaru KK, George E, Wake N, Caterson EJ, Pomahac B, Ho VB, Grant GT, Rybicki FJ (2015) Medical 3D printing for the radiologist. RadioGraphics 35(7):1965–1988
60. Kozakiewicz M, Elgalal M, Loba P, Komuński P, Arkuszewski P, Broniarczyk-Loba A, Stefańczyk L (2009) Clinical application of 3D pre-bent titanium implants for orbital floor fractures. J Craniomaxillofac Surg 37(4):229–234

61. Frame M, Huntley JS (2012) Rapid prototyping in orthopaedic surgery: a user's guide. Sci World J 2012:1–7
62. Kozakiewicz M, Szymor P (2013) Comparison of pre-bent titanium mesh versus polyethylene implants in patient specific orbital reconstructions. Head Face Med 9(1):32
63. Chen, J. *Idea to Implementation: Reimbursement, the Elephant in the Room*. 2017 September 17, 2017]; Available from: http://3dheals.com/idea-implementation-reimbursement-elephant-room/
64. Enquobahrie A, Gobbi D, Turek MW, Cheng P, Yaniv Z, Lindseth F, Cleary K (2008) Designing tracking software for image-guided surgery applications: IGSTK experience. Int J Comput Assist Radiol Surg 3(5):395–403
65. Strong EB, Rafii A, Holhweg-Majert B, Fuller SC, Metzger MC (2008) Comparison of 3 optical navigation systems for computer-aided maxillofacial surgery. Arch Otolaryngol–Head Neck Surg 134(10):1080–1084
66. Gumprecht HK, Widenka DC, Lumenta CB (1999) BrainLab VectorVision Neuronavigation system: technology and clinical experiences in 131 cases. Neurosurgery 44(1):97–104
67. Olson G, Citardi MJ (2000) Image-guided functional endoscopic sinus surgery. Otolaryngol Head Neck Surg 123(3):188–194
68. Hassfeld S, Zöller J, Albert FK, Wirtz CR, Knauth M, Mühling J (1998) Preoperative planning and intraoperative navigation in skull base surgery. J Craniomaxillofac Surg 26(4):220–225
69. Gellrich N-C, Schramm A, Hammer B, Rojas S, Cufi D, Lagrèze W, Schmelzeisen R (2002) Computer-assisted secondary reconstruction of unilateral posttraumatic orbital deformity. Plast Reconstr Surg 110(6):1417–1429
70. Watzinger F, Wanschitz F, Wagner A, Enislidis G, Millesi W, Baumann A, Ewers R (1997) Computer-aided navigation in secondary reconstruction of post-traumatic deformities of the zygoma. J Craniomaxillofac Surg 25(4):198–202
71. Klug C, Schicho K, Ploder O, Yerit K, Watzinger F, Ewers R, Baumann A, Wagner A (2006) Point-to-point computer-assisted navigation for precise transfer of planned zygoma osteotomies from the stereolithographic model into reality. J Oral Maxillofac Surg 64(3):550–559